X-ray linear dichroism dependence on ferroelectric polarization

2012 J. Phys.: Condens. Matter 24 245902

(http://iopscience.iop.org/0953-8984/24/24/245902)

IOP PUBLISHING JOURNAL OF PHYSICS: CONDENSED MATTER
J. Phys.: Condens. Matter **24** (2012) 245902 (7pp) doi:10.1088/0953-8984/24/24/245902

X-ray linear dichroism dependence on ferroelectric polarization

S Polisetty[1], J Zhou[1], J Karthik[2], A R Damodaran[2], D Chen[1], A Scholl[3], L W Martin[2] and M Holcomb[1]

[1] Department of Physics, West Virginia University, Morgantown, WV 26506, USA
[2] Department of Materials Science and Engineering and Materials Research Laboratory, University of Illinois at Urbana–Champaign, Urbana, IL 61801, USA
[3] Advanced Light Source, Lawrence Berkeley National Laboratory, Berkeley, CA 94720, USA

E-mail: srinivas.polisetty@mail.wvu.edu

Received 16 March 2012, in final form 13 April 2012
Published 24 May 2012
Online at stacks.iop.org/JPhysCM/24/245902

Abstract
X-ray absorption spectroscopy and photoemission electron microscopy are techniques commonly used to determine the magnetic properties of thin films, crystals, and heterostructures. Recently, these methods have been used in the study of magnetoelectrics and multiferroics. The analysis of such materials has been compromised by the presence of multiple order parameters and the lack of information on how to separate these coupled properties. In this work, we shed light on the manifestation of dichroism from ferroelectric polarization and atomic structure using photoemission electron microscopy and x-ray absorption spectroscopy. Linear dichroism arising from the ferroelectric order in the $PbZr_{0.2}Ti_{0.8}O_3$ thin films was studied as a function of incident x-ray polarization and geometry to unambiguously determine the angular dependence of the ferroelectric contribution to the dichroism. These measurements allow us to examine the contribution of surface charges and ferroelectric polarization as potential mechanisms for linear dichroism. The x-ray linear dichroism from ferroelectric order revealed an angular dependence based on the angle between the ferroelectric polarization direction and the x-ray polarization axis, allowing a formula for linear dichroism in ferroelectric samples to be defined.

(Some figures may appear in colour only in the online journal)

1. Introduction

Dichroism techniques have been employed in a wide variety of studies—from imaging domains and domain walls in magnetic [1] and magnetoelectric [2, 3] materials to investigating surface and interface effects such as magnetic vortices [4], strain-induced magnetism [5] and exchange coupling [6]. The polarization-dependent absorption that characterizes dichroism originates from anisotropies in the charge or spin of the material [7]. X-ray magnetic circular dichroism (XMCD)—the change in absorption between left and right circularly polarized x-rays (or equivalently between a magnetic field applied in two antiparallel directions)—has been utilized to study ferromagnetism since 1991, when it was first predicted to occur in 3*d* transition metals by van der Laan [8, 9]. Although XMCD is an excellent method for studying ferromagnetism, the technique is not suited for use on an antiferromagnet due to the absence of the imbalanced density of spin states at the Fermi level. In order to characterize antiferromagnetic materials, a second technique—x-ray magnetic linear dichroism (XMLD)—can be employed. This effect, which utilizes x-rays with linear instead of circular polarization, was first applied to examine terbium iron garnet [8]. Since this work, the application of XMLD in determining the antiferromagnetic spin axis of materials such as $LaFeO_3$ and $BiFeO_3$ has brought substantial attention to its potential use in magnetic materials and multiferroics [10–12]. In the case of $BiFeO_3$ (BFO), both magnetic and ferroelectric contributions to the linear dichroism were utilized to understand the effect of epitaxial thin-film strain on the evolution of antiferromagnetic order of this material [5]. Although a ferroelectric contribution

to dichroism had been discussed in the x-ray and optical regions [7, 13], an additional component was verified in linear dichroism related to ferroelectricity as well as magnetism. Failure to account for this ferroelectric contribution to the dichroism may lead to incongruous analysis of linear dichroism in multiferroic and magnetoelectric films. Simultaneously, an exclusive knowledge of ferroelectric ordering is crucial in determining the magnetic properties and potential magnetoelectric coupling of multiferroics and magnetoelectric materials. Additionally, if this ferroelectric contribution to linear dichroism is known, a larger range of systems can be explored through this technique. Therefore, we have studied linear dichroism in a purely ferroelectric material, $PbZr_{0.2}Ti_{0.8}O_3$ (PZT), in order to fully understand the ferroelectric contribution to dichroism.

PZT films were selected for the present study for many reasons: this material is commonly used in technology, there exists a large body of research on the ferroelectric nature of this material, and it is possible to synthesize high-quality thin films with either monodomain or multidomain structures. Recent studies of local x-ray absorption spectroscopy (XAS) on single-domain ferroelectric PZT revealed a pronounced difference at the Ti $L_{3,2}$ absorption edges between the spectra obtained using x-ray polarization parallel and perpendicular to the ferroelectric direction in monodomain samples [14]. Utilizing these differences at the Ti adsorption edge, our study explores the usefulness of XAS and photoemission electron microscopy (PEEM) to understand ferroelectric domains in both single and multiple layers. The following studies illustrate that PEEM is an essential tool to probe local dichroic effects, vital for studies on ferroelectric and multiferroic materials. Our work demonstrates that while a surface charge effect is present, the ferroelectric direction plays the dominant role in the angular dependence of x-ray linear dichroism. Even between in-plane ferroelectric domains (same out-of-plane component), there is a significant difference in the angular dependence. Since dichroism measurements typically involve sample or light polarization rotation, the angular dependence of these contributions must be known to ensure the correct conclusions are reached. The present work explores the angular dependence of the ferroelectric contribution to linear dichroism in PZT films, which will improve the analysis of single and multidomain ferroelectric, multiferroic and magnetoelectric materials via PEEM.

2. Experimental details

A single crystalline $LaAlO_3$ (LAO) (001)-oriented (Crystec GmbH, Berlin) substrate was used to grow the 225 nm PZT/15 nm $La_{0.5}Sr_{0.5}CoO_3$ (LSCO) heterostructure. Bilayers of PZT and LSCO were fabricated using pulsed laser deposition (PLD) with a KrF excimer laser ($\lambda = 248$ nm). The LSCO bottom electrode was deposited at a laser repetition rate of 3 Hz in a background oxygen atmosphere of 100 mTorr at a stable substrate temperature of 650 °C and the PZT was subsequently deposited at 2 Hz in an oxygen atmosphere of 200 mTorr at a substrate temperature of 600 °C. A laser fluence of ∼1.5 J cm^{-2} was used in the synthesis of both layers. After growth, the heterostructures were cooled at a rate of 5 ° C min^{-1} to room temperature at an oxygen pressure of 760 mTorr. A high-resolution x-ray diffraction (XRD) (Philips X'Pert MRD Pro) revealed (figure 1(a)) single-phase, fully 00*l*-oriented, high-quality PZT films. A magnified view of the 002 and 200 diffraction peaks for the tetragonal PZT and 002 diffraction peak of rhombohedral LAO are shown in the inset of figure 1(a). The rocking curves of the 200 and 002 diffraction peaks of PZT were measured to find the percentage of *a*- and *c*-domains, respectively [15]. Based on this analysis, we estimate that these films possess 30%–40% *a*-domains (in-plane (IP) polarized) [16] and 60%–70% *c*-domains (out-of-plane (OOP) polarized) [17]. Atomic force microscopy (AFM) scans (figure 1(b)) reveal a smooth surface with a root-mean-square surface roughness of 0.25 nm. As expected for PZT, the AFM scans revealed surface topographical features corresponding to IP polarized *a*-domains (dark contrast) and OOP polarized *c*-domains (bright contrast). By calculating the percentage of dark and bright contrasts of figure 1(b), we obtained results for the relative fraction of *a*- and *c*-domains in accordance with the XRD results. In addition to uniform single thin films of PZT, we also employed laser MBE-grown double-wedges of $La_{0.7}Sr_{0.3}MnO_3$ (LSMO)/PZT thin films in order to fully understand the ferroelectric contribution to linear dichroism. In this second sample a wedge LSMO film with varying thicknesses of LSMO ($t_{LSMO} \sim$ 0–10 nm) was deposited at an orthogonal direction onto a wedge of PZT film ($t_{PZT} \sim$ 0–300 nm) to confirm the angular dependence of the ferroelectric polarization in multilayer systems, as discussed later. The temperature and pressure for LSMO deposition were 700 °C and 100 mTorr.

In order to accurately determine the angular dependence of the linear dichroism from ferroelectric directions, it is vital to begin with well-characterized ferroelectric domains. The existence of multiple domains in a single sample is an ideal scenario, as the angular dependence may be compared for several ferroelectric domains in a single attempt, ensuring identical normalization procedures. In light of this, PZT samples were selected that exhibit ferroelectric domains along both the OOP (*c*-domains) and IP (*a*-domains) directions. Regions of the PZT/LSCO/LAO thin-film heterostructures were poled using piezoresponse force microscopy (PFM, Cypher, Asylum Research) by applying a bias of 22.5 V between the cantilever tip and bottom electrode within the area in the dotted box in figure 1(c). The phase of the vertical piezoresponse (relative to the applied voltage signal on the cantilever tip) revealed contrast between regions with downward/upward pointing polarization components. The IP PFM image (figure 1(c)) displayed two contrasts; dark cross-hatched patches corresponding to the *a*-domains and the bright background regions corresponding to *c*-domains. The violet color within the box of the inset of figure 1(c) shows the poled area of OOP PFM image. A three-dimensional view of the sample geometry (figure 1(d)) is provided to show the relative relation of the domain structure to the crystallographic axes of the system. Furthermore, the PFM illustrates that we have ferroelectric domains with polarization directions

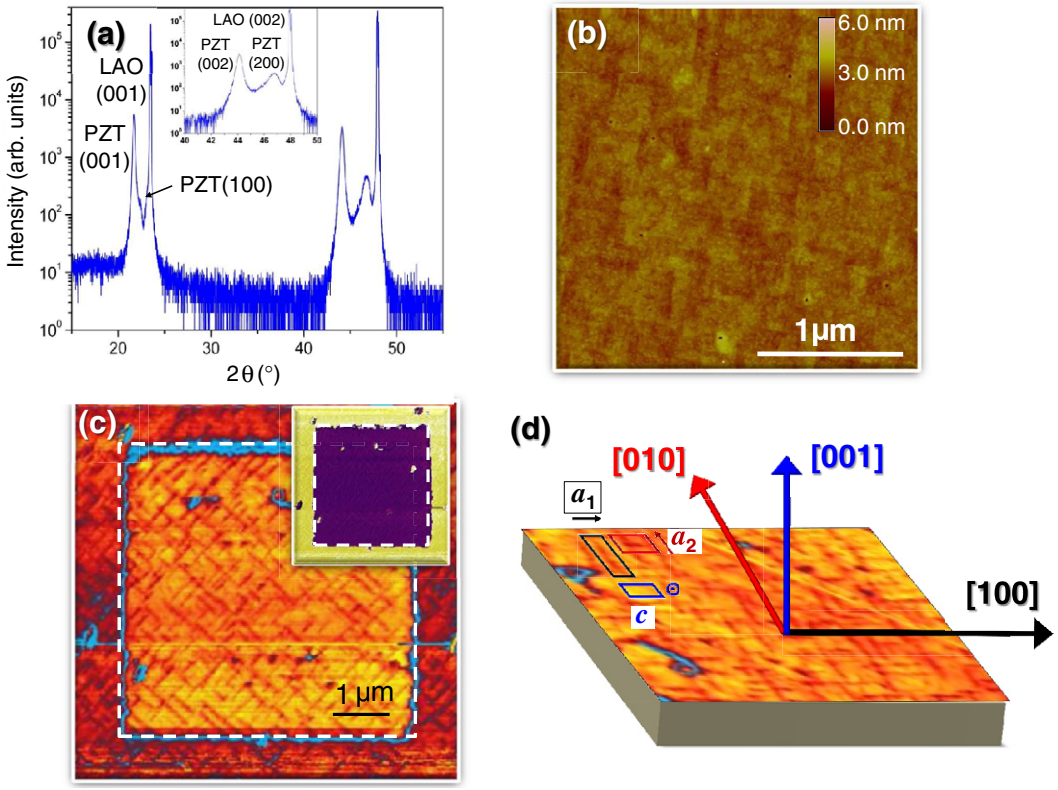

Figure 1. (a) X-ray diffraction pattern of PZT/LSCO/LAO heterostructure. The XRD peaks represent the preferred orientation of tetragonal PZT (00*l*) on the substrate of rhombohedral LAO (001). The inset shows a magnified view of the secondary peaks 002 and 200 of PZT and 002 of LAO. (b) An AFM topology image of PZT over a 2.5 μm × 2.5 μm area illustrates smooth films. (c) PFM image of in-plane projections of the ferroelectric domains. The inset shows PFM image of the electrically poled out-of-plane projections of the same location. (d) Three-dimensional representation of poled area on the sample. Bright regions are the out-of-plane ferroelectric polarization oriented along [001], as indicated by blue box. The in-plane ferroelectric directions are oriented along [100] and [010] directions, as indicated black and red boxes.

pointing along these same directions. The *c*-domains (bright regions as shown in the blue colored box in figure 1(d)) are polarized along the [001] and the a_1- and a_2-domains (dark regions as shown in the black and red boxes in figure 1(d)) are polarized along the [100] and [010], such that the domains have head-to-tail alignment and the domain wall is parallel to the {101} of the substrate [16, 18]. This model ferroelectric domain structure forms the reference frame for study of the contribution of ferroelectric polarization to linear dichroism and PEEM measurements.

Soft XAS and PEEM experiments were performed using linearly polarized light provided by beamlines 6.3.1 and 11.0.1 at the Advanced Light Source, Lawrence Berkeley National Laboratory. The incident x-rays were directed at an angle of 30° with respect to the sample surface. The photoemitted electrons from the sample were extracted into an electro-optical imaging system by an electric field applied between the sample and the electro-optical system. The absorption spectra for these electrons depend on anisotropies in the charge and thus are sensitive to the relative orientation of the x-ray polarization and ferroelectric axes, which are imaged by PEEM. XAS of the Ti L-edge of the PZT sample (figure 2(a)) were measured at room temperature for incident x-rays with polarization in the plane (solid green curve) and out of the plane (dotted pink curve) over an area 50 μm × 50 μm of the PZT film. Figure 2(b) is the x-ray linear dichroism data obtained by subtracting out-of-plane XAS data ($\alpha = 0°$) from in-plane data ($\alpha = 90°$) of figure 2(a). As shown in figure 2(b), the maximum dichroism was observed at the shoulder of the L_{3A}-absorption edge. Therefore, subsequent PEEM imaging (acquisition time = ∼10 h) was completed at ± 0.15 eV from the Ti L_{3A}-absorption edges and further divided for each polarization of the incident x-ray, as is the standard method of analyzing domains by PEEM [19]. The intensities discussed below are the contrast of these divided images.

Figure 3(a) shows a schematic illustration of the incident x-rays and the x-ray polarization axes with reference to the sample. Pink and green double arrows in figure 3(a) indicate the polarization axes of the incident x-rays when $\alpha = 0°$ (i.e., x-ray polarization at an angle of 30° from the normal to the surface of the sample) and $\alpha = 90°$ (i.e., the x-ray polarization lies in the plane of the sample). The three thick arrows (black, red and blue) in figure 3(a) denote the ferroelectric polarization directions present in the PZT sample. The divided PEEM images of the same poled area of a PZT sample for incident x-ray polarizations with $\alpha = 0°$, 40°, 60° and 90° are shown in figures 3(b)–(e), respectively. For all these cases, the x-rays originate from the right side of the PEEM images, as

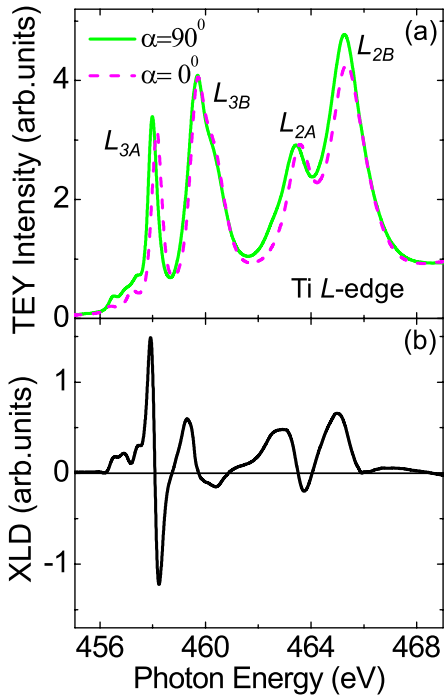

Figure 2. (a) X-ray absorption spectroscopy of the Ti L-edge obtained over 50 μm × 50 μm for a typical PZT sample. Dotted pink and solid green curves belong to the incident x-ray polarizations, $\alpha = 0°$ (p-polarized) and $\alpha = 90°$ (s-polarized). (b) X-ray linear dichroic spectrum showing maximum dichroism at $L_{3A} \pm 0.15$ eV.

illustrated in figure 3(e). As expected, the PEEM images 3(b) and (e) resemble the PFM image (figure 1(c)).

3. Results and discussion

The intensities of the ferroelectric a_1, a_2 and c domains (i.e., [100], [010] and [001]) from the divided PEEM images were measured for all polarizations of incident x-rays using image analysis masks to separate contrasts for different domains. Figure 3(f) is the result of a comparison of the intensity of the divided dichroic images versus x-ray polarization from the three different ferroelectric directions in the PZT samples. The upwards and downwards pointing triangles correspond to the intensity values of ferroelectric directions of the a_1- and a_2-domains, respectively. The circles represent the intensity profile of the ferroelectric directions of the c-domains. As the polarization of the incident x-rays rotates from $\alpha = 0°$ to 90°all three domains reverse contrast (bright to dark and vice versa). For example, at $\alpha = 0°$ cross-hatched a_1, a_2-domains appear bright whereas c-domains appear dark, as shown by the boxes in figure 3(b). When the polarization of incident x-rays rotates to $\alpha = 40°$, the brightness of a_2-domains is reduced, as shown in figure 3(c). This intensity reduction causes only the a_1-domains to appear bright in contrast. With further rotation of x-ray polarization to $\alpha = 60°$, both a_1- and a_2-domains appear darker and the c-domains brighter, as displayed in figure 3(d). These effects combine to highlight only the a_2-domains with dark contrast. Finally, for $\alpha = 90°$, a_1-, a_2- and c-domains demonstrate the opposite contrast from what was observed at $\alpha = 0°$. By analyzing the change in contrast for all the ferroelectric domains as the x-ray polarization is rotated, the angular dependence and mechanism behind the ferroelectric linear dichroism can be determined.

To investigate the angular dependence of the ferroelectric order, we start with the polarization axis of the incident x-rays at $\alpha = 0°$. For this angle, the ferroelectric a_1- and a_2-domains make a projection of $(\cos 60°)$ $(\cos 45°)$ onto the polarization of the incident x-rays. The ferroelectric c-domains make a projection of $\cos 30°$ with the x-ray polarization axis, as shown in figure 3(a). Thus, the intensity of the ferroelectric polarization from a_1- and a_2-domains should have the same value and c-domains should have a different intensity, as observed in the boxes of figure 3(b). Linear dichroism can be expected to follow a cosine squared relation due to the use of linearly polarized x-rays [14]. Thus, antiparallel directions will have the same projection onto the x-ray polarization axis and a rotation of 90° in x-ray polarization should result in a reversal of contrast. If the angular dependence of the ferroelectric contribution were proportional to the square of the projections of the ferroelectric directions onto the x-ray polarization axis, the intensity values of a_1, a_2-domains and c-domains should have $(\cos 60° \cos 45°)^2 = 0.125$ and $\cos^2 30° = 0.75$. A similar result is observed, as shown in figure 3(f). The intensity values obtained from ferroelectric a_1, a_2-domains and c-domains are comparable to one minus the projection squared, or $1 - (\cos 60° \cos 45°)^2 = 0.875$ and $1 - \cos^2 30° = 0.25$, correspondingly for $\alpha = 0°$. Additional insight is gained by considering the polarization axis of the x-rays in the plane of the sample ($\alpha = 90°$). For this angle, the ferroelectric polarization directions of the a_1- and a_2-domains make a projection of $\cos 45°$ with respect to the polarization of the incident x-rays and, thus, the domains appear dark in the dichroic PEEM images shown in figure 3(e). For the same angle of α, the ferroelectric directions of c-domains are perpendicular to the polarization of the incident x-rays and thus are expected to exhibit minimum intensity in figure 3(f) if the angular dependence of the ferroelectric contribution is proportional to the projections of the ferroelectric directions onto the x-ray polarization axis. From figure 3(f), however, the reverse is again observed; both a_1- and a_2-domains have the same intensity ($\sim 1 - \cos^2 45° = 0.5$), and the c-domains have maximum intensity ($\sim 1 - \cos^2 90° = 1$).

With the help of a series of images, as well as analysis of the corresponding geometries and angles, we extracted the angle dependence of the dichroic contrast for all three ferroelectric polarizations present in the sample. The results are shown in figure 3(g). The angular dependence of the ferroelectric polarization to the linear dichroism has been modeled as

$$I = (1 - \cos^2 \theta_{FE}) \langle P^2 \rangle_T, \quad (1)$$

where P is the ferroelectric polarization at a temperature T and θ_{FE} is the angle between the ferroelectric direction and the polarization axis of the incident x-rays. θ_{FE} can be shown to be related to the polarization axis of the incident x-rays, α. For example, for a_1-domains at the sample geometry shown in figure 3(a), $\theta_{FE} = \frac{1}{\sqrt{2}}(\sin(\alpha) - \frac{1}{2}\cos(\alpha))$. Upon inspection,

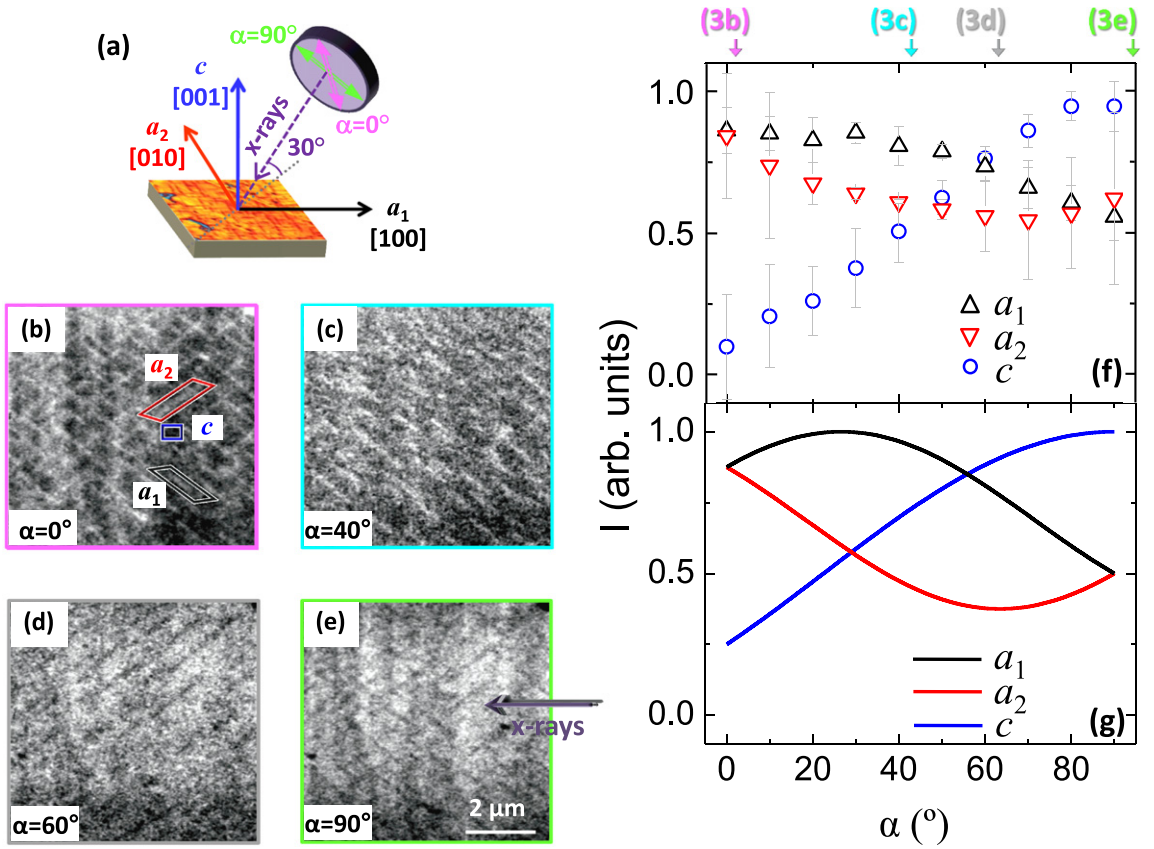

Figure 3. The schematic (a) represents the ferroelectric directions of the PZT and polarization axes of the incident x-rays. The divided dichroic PEEM images were taken at the shoulder of the Ti L_{3A}-edge when the x-ray polarization axes, α, were (b) 0°, (c) 40°, (d) 60° and (e) 90°. The violet arrow on (e) shows the direction of incident x-ray on PEEM images. Frame (f) shows the intensity values from the PEEM images versus x-ray polarization of three different ferroelectric directions; [100], [010] and [001], of a PZT sample and the predicted angular dependence of equation (1) is represented in frame (g).

the angular dependence of figure 3(f) follows the cosine squared model fits in figure 3(g). This cosine squared angular dependence of the ferroelectrics has already been used in multiferroic systems to interpret the magnetic behavior [5]. The results presented here are direct experimental evidence of the cosine squared angular dependence of the ferroelectric polarization contribution to linear dichroism.

To verify the angular dependence of equation (1), the sample was rotated 45° about the normal of the sample while maintaining the same angle of x-ray incidence (i.e., 30° with the surface of the sample). In this new geometry, the x-rays intersect the ferroelectric directions of a_1-domains at an angle of 30° as shown in the figure 4(a). The PEEM images at the L_{3A}-absorption edge in figure 4 were captured by varying the polarization axis of the incident x-ray from $\alpha = 0°$ to 90°, as previously demonstrated in figure 3. Three divided PEEM images are shown in figures 4(b)–(d) for incident polarization, $\alpha = 0°$, 50° and 90°, respectively. The bright orthogonal patches correspond to the ferroelectric directions of a_1 and a_2-domains and the dark contrast between them is the ferroelectric directions of c-domains, as shown in figure 4(b). The three ferroelectric directions are indicated by the boxes in figure 4(d). For this case of sample rotation, x-rays were incident diagonally to the PEEM images, as shown in figure 4(d). Figure 4(e) shows the intensity profiles of three polarization directions in a PZT sample versus α and figure 4(f) presents the predicted angular dependence of equation (1).

For $\alpha = 0°$ (figure 4(b)), the ferroelectric directions of the a_2-domains are now perpendicular to the polarization of the x-rays. In this case, the ferroelectric directions of the a_1- and c-domains make projections onto the x-ray polarization of cos 60° and cos 30°, respectively. If the angular dependence of the ferroelectric contribution is again expected to be given by 1-(projection)^2, the ferroelectric directions of the a_1- and c-domains should produce intensities of $1 - \cos^2 60°$ and $1 - \cos^2 30°$ at this angle. Also, the intensity of the ferroelectric polarization from the a_2-domains should have a maximum intensity. This observation at $\alpha = 0°$ is consistent with the expected predictions of figure 4(f). For the incident x-ray polarization $\alpha = 50°$, all ferroelectric domains make similar projections onto α. Thus, figure 4(c) shows virtually no cross-hatch pattern due to the similar intensities by all ferroelectric domains. When the incident x-ray polarization is rotated to $\alpha = 90°$ (figure 4(d)), the ferroelectric direction of the a_2-domains is parallel to the polarization of the incident x-rays. For the same angle, the ferroelectric polarization of the a_1- and c-domains are perpendicular to the polarization

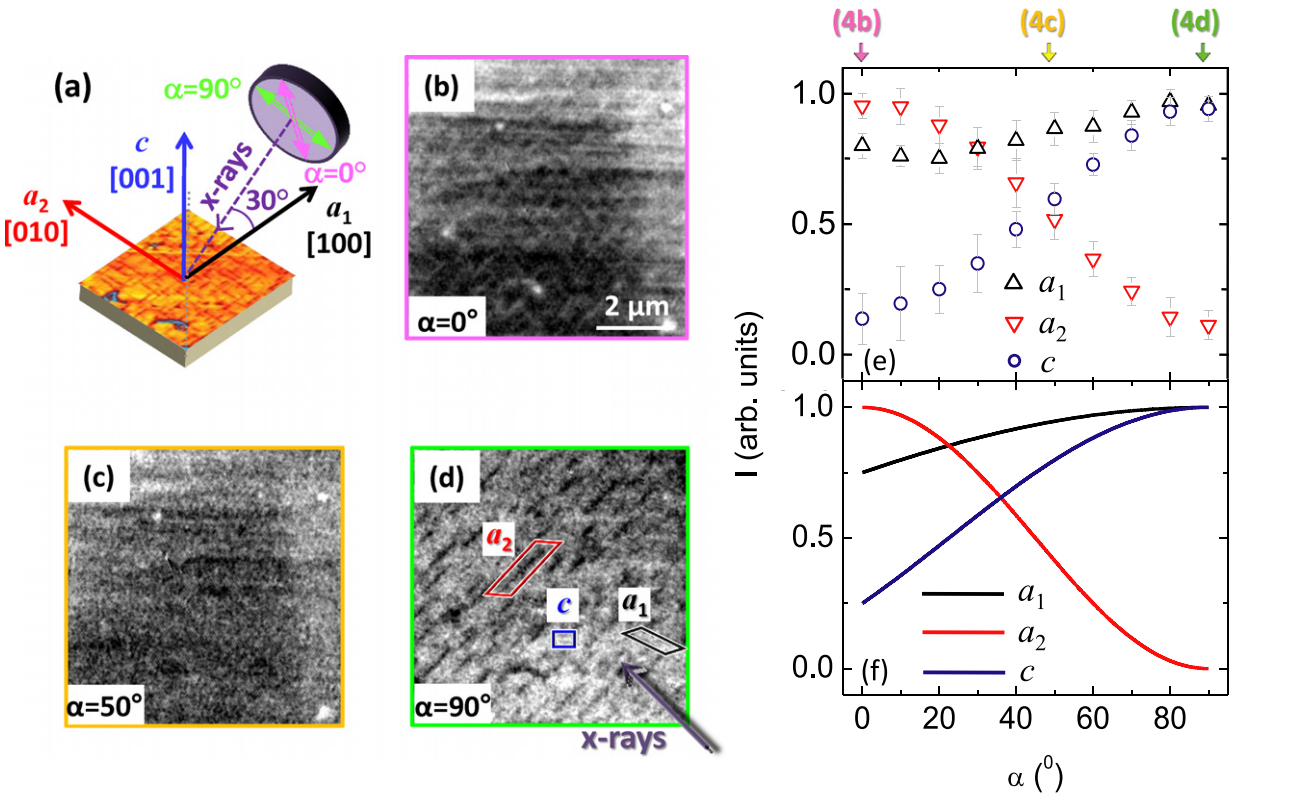

Figure 4. The schematic (a) represents the ferroelectric directions of the PZT and polarization axes of incident x-rays when the sample is rotated by 45° with respect to its normal. The violet arrow on (d) shows the direction of incoming x-rays on PEEM images. Frames (b), (c) and (d) are the corresponding PEEM images for the incident x-ray polarizations, $\alpha = 0°$, 50° and 90°, respectively. (e) Intensity profile of all ferroelectric polarizations present in the sample versus incident x-ray polarization and (f) the predicted angular dependence.

of the incident x-rays. If the angular dependence of the ferroelectric contribution follows the predictions based on their projections onto the x-ray polarization axis, then it would be expected that the ferroelectric directions of a_1- and c-domains should have maximum intensity and the ferroelectric direction of a_2-domains should exhibit minimum intensity in the dichroism image corresponding to this angle. From figure 4(f), the matching features are observed for this angle of $\alpha = 90°$. In addition to $\alpha = 0°$ and 90°, it is evidenced in figure 4(e) that all ferroelectric directions in the PZT sample follow closely to the expected angular dependence of equation (1), as shown in figure 4(f).

Equation (1) was also verified for the Ti L_{3B}-absorption edge, at different thicknesses of PZT and in the bilayer system of ferroelectric/ferromagnetic LSMO/PZT thin films (data not shown). The obtained results confirmed the universal nature of the angular dependence of the ferroelectric polarization. Early predictions of ferroelectric effects on XAS [7] suggested that only surface charges on ferroelectric materials needed to be considered. At the top surface of ferroelectric domains, uncompensated charge will create an effective voltage. As a voltage is required to direct the electrons through the PEEM electro-optics, this effective voltage from the sample may influence the efficiency of this process. While an out-of-plane effect from surface charge was observed through changes in the image contrast in this study, a true ferroelectric origin to linear dichroism was also realized [14]. This is most clearly demonstrated by considering the in-plane domains, which should have identical surface charge since the out-of-plane projections of the ferroelectric directions are identical. However, two distinct angular dependences were observed for in-plane [100] and [010]-ferroelectric domains, as seen in figures 3 and 4.

These results demonstrate that x-ray linear dichroism spectroscopy, in combination with PEEM, is a viable technique to image the ferroelectric domain structure of both surfaces and interfaces, in a manner similar to XMCD–PEEM [20, 21] for ferromagnets and XMLD–PEEM [22, 23] for antiferromagnets. X-ray linear dichroism–PEEM of ferroelectrics provides elemental specificity, surface and buried layer sensitivity (5–10 nm sampling depth) and spatial resolution (∼20 nm) that may not be possible in other ferroelectric imaging techniques, such as piezoresponse force microscopy, scanning electron microscopy, scanning force microscopy, x-ray diffraction and nonlinear second-harmonic generation. When the geometry of the sample and relative angles with respect to the polarization of the incident x-rays are known, the expected outcomes of experiments can be computed, allowing the determination of the ferroelectric directions and the ability to resolve ferroelectric order parameters from magnetic order parameters in magnetoelectric and multiferroic materials. PEEM is the only technique that can perform *in situ* imaging of ferromagnetic, antiferromagnetic and ferroelectric

contributions in magnetoelectric and multiferroic materials without removing the sample from vacuum.

4. Conclusions

The present study illustrates the use of x-ray photoemission electron microscopy for obtaining detailed surface mesoscopic information on the ferroelectric $PbZr_{0.2}Ti_{0.8}O_3$. Images of Ti L_3-absorption edges were collected by continuously changing the polarization of the incident x-rays. The linear dichroism intensity resulting from different ferroelectric directions revealed a cosine squared dependence as a function of incident x-ray polarization, rather than simple surface charge effects. Further imaging of ferromagnetic/ferroelectric bilayers and different thicknesses of ferroelectric material confirmed the universal applicability of the expected cosine squared angular dependence of the ferroelectric polarization in multilayer systems. This development allows the present dynamic approach to be used to investigate the effect of ferroelectricity on layer and interface coupling in a wide range of systems, such as magnetoelectric multiferroics, magnetic materials and capped ferroelectric multilayers. Finally, this work further encourages the broad use of imaging techniques based on x-ray dichroism in a wide range of material systems involving complex order parameters, as novel information can be obtained.

Acknowledgments

We thank Cameron Keenan and David Lederman for their help with additional atomic force microscopy measurements. We acknowledge use of the WVU Shared Research Facilities and Advanced Light Source at Lawrence Berkeley National Laboratory. At UIUC, JK and LWM acknowledge support from the Office of Naval Research under grant N0014-10-1-0525 and ARD and LWM acknowledge support from the Army Research Office under grant W911NF-10-1-0482. Experiments at UIUC were carried out in part in the Frederick Seitz Materials Research Laboratory Central Facilities. We also acknowledge the group of Professor Ying-Hao Chu for providing high-quality double-wedged samples to verify the ferroelectric contribution that could be measured through a thin layer of LSMO.

References

[1] Kottler V, Essaidi N, Ronarch N, Chappert C and Chen Y 1997 *J. Magn. Magn. Mater.* **165** 398
[2] Zimmermann A S, Van Aken B B, Schmid H, Rivera J P, Li J, Vaknin D and Fiebig M 2009 *Eur. Phys. J.* B **71** 355
[3] Zhao T, Scholl A, Zavaliche F, Lee K, Barry M, Doran A, Cruz M P, Chu Y H, Ederer C, Spaldin N A, Das R R, Kim D M, Baek S H, Eom C B and Ramesh R 2006 *Nature Mater.* **5** 823
[4] Vansteenkiste A, Chou K W, Weigand M, Curcic M, Sackmann V, Stoll H, Tyliszczak T, Woltersdorf G, Back C H, Schütz G and Van Waeyenberge B 2009 *Nature Phys.* **5** 332
[5] Holcomb M B, Martin L W, Scholl A, He Q, Yu P, Yang C H, Yang S Y, Glans P A, Valvidares M, Huijben M, Kortright J B, Guo J, Chu Y H and Ramesh R 2010 *Phys. Rev.* B **81** 134406
[6] Schneider C M, Meinel K, Kirschner J, Neuber M, Wilde C, Grunze M, Holldack K, Celinski Z and Baudelet F 1996 *J. Magn. Magn. Mater.* **162** 7
[7] Stöhr J and Siegmann H C 2006 *Magnetism: From Fundamentals to Nanoscale Dynamics, Springer Series in Solid-State Sciences* vol 152 (New York: Springer) pp 401–6
[8] van der Laan G, Thole B T, Sawatzky G A, Goedkoop J B, Fuggle J C, Esteva J M, Karnatak R C, Remeika J P and Dabkowska H A 1986 *Phys. Rev.* B **34** 6529
[9] van der Laan G 1998 *Phys. Rev.* B **57** 5250
[10] Lüning J, Nolting F, Scholl A, Ohldag H, Seo J W, Fompeyrine J, Locquet J P and Stöhr J 2003 *Phys. Rev.* B **67** 214433
[11] Seo J W, Fullerton E E, Nolting F, Scholl A, Fompeyrine J and Locquet J P 2008 *J. Phys.: Condens. Matter* **20** 264014
[12] Arenholz E, van der Laan G, Chopdekar R V and Suzuki Y 2007 *Phys. Rev. Lett.* **98** 197201
[13] Tsuboi T 1989 *Phys. Rev.* B **39** 2842
[14] Arenholz E, van der Laan G, Fraile-Rodríguez A, Yu P, He Q and Ramesh R 2010 *Phys. Rev.* B **82** 140103(R)
[15] Nagarajan V, Jenkins I G, Alpay S P, Li H, Aggarwal S, Salamanca-Riba L, Roytburd A L and Ramesh R 1999 *J. Appl. Phys.* **86** 595
[16] Ganpule S, Nagarajan V, Li H, Ogale A S, Steinhauer D E, Aggarwal S, Williams E, Ramesh R and Wolf P D 2000 *Appl. Phys. Lett.* **77** 292
[17] Alpay S P, Nagarajan V, Bendersky L A, Vaudin M D, Aggarwal S, Ramesh R and Roytburd A L 1999 *J. Appl. Phys.* **85** 3271
[18] Vrejoiu I, Le Rhun G, Zakharov N D, Hesse D, Pintilie L and Alexe M 2006 *Phil. Mag.* **86** 4477
[19] Stöhr J, Scholl A, Regan T J, Anders S, Lüning J, Scheinfein M R, Padmore H A and White R L 1999 *Phys. Rev. Lett.* **83** 1862
[20] Imada S, Suga S, Kuch W and Kirschner J 2002 *Surf. Rev. Lett.* **9** 877
[21] Taniuchi T, Yasuhara R, Kumigashira H, Kubota M, Okazaki H, Wakita T, Yokoya T, Ono K, Oshima M, Lippmaa M, Kawasaki M and Koinuma H 2007 *Surf. Sci.* **601** 4690
[22] van der Laan G, Telling N D, Potenza A, Dhesi S S and Arenholz E 2011 *Phys. Rev.* B **83** 064409
[23] Duò L, Brambilla A, Biagioni P, Finazzi M, Scholl A, Gweon G H, Graf J and Lanzara A 2006 *Surf. Sci.* **600** 4160